THE ASTROPHYSICAL JOURNAL, 356:389–398, 1990 June 20

THE STRUCTURE AND IONIZATION OF THE EXTENDED EMISSION-LINE FILAMENTS SURROUNDING THE QSO MR 2251−178[1]

F. MACCHETTO,[2] L. COLINA,[2] AND D. GOLOMBEK
Space Telescope Science Institute
M. A. C. PERRYMAN
Astrophysics Division, Space Science Department of ESA
AND
S. DI SEREGO ALIGHIERI[2]
Space Telescope European Coordinating Facility, Garching
Received 1989 September 14; accepted 1989 December 21

ABSTRACT

New and deep high spatial resolution images of the QSO MR 2251−178 in the [O II] λ3727, [O III] λ5007, and Hα emission lines together with VLA radio maps are presented.

The VLA radio maps show MR 2251−178 as a weak extended radio source with a double-sided radio jet structure, i.e., Fanaroff-Riley class I galaxy. Also the nearby galaxy G1 located to the north at a projected distance of 75 kpc has been detected at both 6 and 20 cm as an unresolved source at the present resolution.

The quasar MR 2251−178 is a unique example of weak radio source showing an extended system of emission-line filaments surrounding it. The size, luminosity, excitation conditions, and mass of the ionized gas is similar to that detected around very powerful radio sources at low and high redshift.

Circumnuclear emission-line gas is detected for the first time in [O II] λ3727 and [O III] λ5007. This ionized gas is located at distances between 3 and 6 kpc from the nucleus and is consistent with gas directly ionized by the central nonthermal source. These regions are strongly concentrated around the radio axis in the same way as is observed in some nearby Seyfert galaxies and high-redshift radio galaxies.

Two new systems of Hα filaments are also observed for the first time. These systems are located at distances of 30 kpc and 50 kpc to the east of the MR 2251–178 nucleus and have a circular filamentary structure with a total size of almost 70 kpc and 100 kpc, respectively. An upper limit of $9.3 \times 10^9\ M_\odot$ and $2.1 \times 10^{10}\ M_\odot$ has been derived for the amount of ionized gas in these filaments.

Several high-excitation emission-line filaments have been detected in the [O III] λ5007 emission line around MR 2251−178 forming, together with the Hα filaments, a ring structure at a radial distance of 50 kpc. The upper limit for the mass in these filaments is $2 \times 10^9\ M_\odot$ and the ionization parameter is similar to that found in the extended emission line regions (EELR) around nearby radio galaxies.

Two possible scenarios consistent with the observations are outlined. One is the interaction between MR 2251−178 and the galaxy G1. The second one considers MR 2251−178 and the system of filaments as the merger result of a giant elliptical with a smaller disk galaxy.

Subject headings: galaxies: individual (MR 2251−178) — galaxies: interactions — galaxies: nuclei — quasars — radio sources: galaxies

I. INTRODUCTION

MR 2251−178, $z = 0.06398$ (Bergeron *et al.* 1983), was first discovered by Ricker *et al.* (1978) on the basis of its strong X-ray emission, $\log L(2\text{–}10\ \text{keV}) = 45.0\ \text{ergs s}^{-1}$; it was consequently classified as a quasar.

Variations in the spectrum have been observed on time scales ranging from one month to one year both in the optical (Ricker *et al.* 1978) and ultraviolet (Bergeron *et al.* 1983). X-ray variations by a factor of 10 have also been detected (Cooke *et al.* 1978).

The radial luminosity profile of MR 2251−178 has been studied by Hutchings and collaborators (Hutchings and Campbell 1983; Hutchings *et al.* 1984). They found an asymmetric light distribution with a broad tail connecting MR 2251−178 with the companion galaxy north of it.

MR 2251−178 lies within a small group of galaxies and is surrounded by an extended ionized envelope (Bergeron *et al.* 1983). This envelope has been studied using long-slit spectrophotometry (Bergeron *et al.* 1983) and direct imaging through [O III] λ5007 narrow-band filters (Hansen, Nørgaard-Nielsen, and Jorgensen 1984; di Serego Alighieri, Perryman, and Macchetto 1984; Nørgaard-Nielsen *et al.* 1986). These studies show that the galaxy housing MR 2251−178 is an elliptical galaxy with a magnitude $M_v = -22.5$ (Nørgaard-Nielsen *et al.* 1986). Some indications of a rotational velocity pattern have been detected in the extended envelope (Bergeron *et al.* 1983; although see Nørgaard-Nielsen *et al.* 1986), suggesting that the ionized envelope is bound to MR 2251−178.

The origin and excitation of the ionized gas is still unclear. Several possibilities involving intergalactic gas or tidally stripped gas from the surrounding galaxies have been pro-

[1] Based on observations collected at ESO, CFHT, and VLA. The CFHT is operated by the National Research Council of Canada, the Centre National de la Recherche Scientifique of Frannce, and the University of Hawaii; the VLA is operated by the Associated Universities, Inc., under contract with the National Science Foundation.

[2] Affiliated with the Astrophysics Division, ESTEC, Noordwijk, The Netherlands.

posed. This gas could be ionized by the hard UV radiation generated in the nucleus of MR 2251−178 (see previous references).

In the following we present new VLA radio maps at 6 cm and 20 cm together with deep high spatial resolution maps in the [O II] λ3727, [O III] λ5007, and Hα light. The morphology of the circumnuclear emission-line regions and the extended system of filaments in different ionization states are shown. The physical characteristics like luminosities, densities, mass, and ionization parameters are derived for the different filaments. Explanation of the excitation conditions is given in terms of a hard UV nonthermal source located in the nucleus of MR 2251−178. Two overall scenarios to explain the origin of the gas filaments and the generation of the nonthermal source in terms of interaction or merging with small galaxies are outlined.

Throughout the paper a Hubble constant $H_0 = 50$ km s^{-1} Mpc^{-1} will be used. One arcsecond corresponds to 1.9 kpc.

II. OBSERVATIONS AND REDUCTIONS

a) Optical Observations

Narrow-band images of MR 2251−178 were obtained at the Cassegrain focus of the Canada-France-Hawaii telescope on 1984 October with the ESA photon counting detector (PCD). This detector, the prototype for the faint object camera (FOC) for the *Hubble Space Telescope*, is described in di Serego Alighieri, Perryman, and Macchetto (1985). The image format used was 512 by 512 pixels with pixel sizes of 50 μm by 50 μm or 25 μm by 25 μm, having scales of 0".31 and 0".155 per pixel, respectively. These configurations will be noted as corresponding to the "zoom" and "unzoomed" images.

Images were obtained at the redshifted wavelengths of Hβ, [O III] λ5007, and [O II] λ3727 using narrow-band interference filters. The corresponding narrow-band continuum images were centered at rest wavelengths λ3730, λ5000, and λ5100. Using the same configurations and set of filters, the white dwarf Feige 24 was observed as a calibration standard. The log of the observations is detailed in Table 1.

Seeing conditions were determined by fitting Gaussian profiles to the stars in the field of the zoomed images. Typical values of the FWHM were between 0".7 and 1".

On 1986 July using the ESO faint object spectrograph and camera (EFOSC) on the ESO 3.6 m telescope broad-band *V* and redshifted Hα CCD images were obtained (see Table 1). The CCD used was the thinned back-illuminated RCA chip no. 3. The pixel size of 30 μm corresponded to 0".675 on the sky and the images were 320 by 512 pixels in size after processing to remove an overscan region. Dome flat fields were obtained using the same configuration. A set of dark frames was also taken during the run. For absolute calibration, the standard LTT 7379 was also observed with the same filters. Seeing conditions were determined in the same way as for the PCD images, giving a typical FWHM of 1".5.

b) Radio Observations

Radio observations with the VLA at 20 and 6 cm were made in 1985 March and August, respectively (see Table 1). The A/B hybrid configuration was used for the 20 cm observation, with a beam of 3".41 by 1".83 FWHM and the major axis of the beam at P.A. 79°. The 6 cm observations were made with the C-configuration. In this case the beam was 5".38 by 2".95 FWHM and the major axis lies at P.A. 175°.

c) Reductions

The PCD images display the typical distortions of magnetically focused intensifiers as well as a nonperpendicularity between the horizontal and vertical scan directions. To correct for these distortions, fiducial marks are made at the photocathode of the instrument. These reseau marks are used to generate a grid and geometrically correct the images. These corrections were made using FOC data reduction tasks, part of STSDAS written at Space Telescope Science Institute (STScI). No reseaux marks were found in some of the images with very low count rate. In these cases, we used positions found in the (temporally) closest image with marks. The flat-field images were also geometrically corrected, and the reseaux were removed by interpolating with close neighbors. Once the images were geometrically correct, they were divided by the appropriate flat. Line images were created by substracting the continuum once aligned and after appropriate signal scaling. When there was a difference in seeing between the line and the continuum images, we smoothed to the worse of both before the subtraction was made. The scaling factors were obtained considering the PCD plus filter efficiency, integration time and filter bandpass. These factors agree within 10%–15% with those obtained from the background counts.

To check the precision of our absolute calibration, we compare the [O III] λ5007 flux within the nucleus of MR

TABLE 1

OPTICAL AND RADIO OBSERVATIONS OF MR 2251−178

Date	Telescope	Instrument	Line	Filter Å/Å	Exposure Time (minutes)	Comment
1984 Oct 16	CFHT	PCD	[O II] λ3727	3970/40	15	zoom
			[O II] λ3727	3970/40	30	
			continuum	3730/120	10	
			[O III] λ5007	5330/40	10	
			continuum	5100/100	10	
1984 Oct 18	CFHT	PCD	Hβ	5200/100	30	
			[O III] λ5007	5300/40	60	zoom
			continuum	5000/100	20	zoom
1986 Jul 7	ESO 3.6 m	EFOSC	continuum	*V*	10	
			Hα	6956/64	25	
1985 Mar 23	VLA	A/B configuration	20 cm		248	
1985 Aug 19	VLA	C configuration	6 cm		238	

2551 − 178 with the values obtained by Bergeron *et al.* (1983) and Hansen, Nørgaard-Nielsen, and Jorgensen (1984). Also an internal calibration could be obtained comparing the flux in our zoomed and unzoomed [O III] λ5007 images. We conclude that fluxes in our zoomed [O III] λ5007 image could be underestimated by a factor of 2 although the uncertainties in Bergeron *et al.* (1983) and Hansen, Nørgaard-Nielsen, and Jorgensen (1984) are also large. In addition, the internal calibration indicates that the absolute calibration has an uncertainty of a factor of 2. For the [O II] λ3727 no standard star was available, and the absolute calibration was derived by comparing our raw counts in the nucleus with the flux obtained by Bergeron *et al.* (1983) within a slit of 3″ by 5″.3 around the nucleus.

The EFOSC CCD images were corrected for bias level, dark subtracted, and flat fielded using normal techniques. The bias was determined from the mean counts in the overscan region. Darks and flats were taken during the run. As the broad-band flats were found to be faulty, a new set was taken and sent to us by ESO. These new flats were combined and median filtered with a 19 by 19 pixel box.

The Hα and *V* aligned images were subtracted after appropriate scaling. Although the Hβ and [O III] lines lie within the band of the *V* filter, no correction for the effect of these lines in the *V* light distribution was made. We believe that this effect is only important in the nucleus of MR 2251 − 178 where the bright and broad Hβ line is observed. In the outer and extended envelopes the effect is negligible since the Hβ emission line is not observed outside the nucleus and most of the [O III] extranuclear filaments are not spatially coincident with the Hα filaments. Also the surface brightness of these filaments is less than 1%–2% of the *V* sky background (no indication of any extended emission is present in our *V* image).

All final PCD and EFOSC differential images were reorientated in order to have north at the top and east at left. These true positions were found by inspection of an astrometric image of the field provided to us by the Guide Star Group at STScI.

The atmospheric extinction correction was performed by measuring the air mass for each particular exposure and using the mean extinction curves of La Silla (ESO User's Manual) and Mauna-Kea (Mauna-Kea User's Manual) observatories. Since the absolute value of the galactic latitude of MR 2251 − 178 is larger than 50° ($b = -61°.3$), no correction for the interstellar extinction within our galaxy has been considered.

II. RESULTS

a) The Radio Structure

Our VLA observations of MR 2251 − 178 at 20 cm (see Fig. 1*a*) and 6 cm (see Fig. 1*b*) show it to be an extended weak radio source with total luminosities log *L* (6 cm) = 23.11 W Hz^{-1} and log *L* (20 cm) = 23.38 W Hz^{-1} (see Table 2 for details). Therefore it is a flat spectrum radio source with a spectral index $\alpha_{20}^{6} = 0.52$ ($F_\nu \propto \nu^{-\alpha}$). These values agree with the results of Kembhavi, Feigelson, and Singh (1986). They obtained from VLA observations with the B-configuration, core luminosities log *L* (6 cm) = 22.79 W Hz^{-1} and log *L* (20 cm) = 23.01 W Hz^{-1} with a spectral index $\alpha_{20}^{6} = 0.50$.

The VLA 20 cm radio map (see Fig. 1*a*) shows an elongated jetlike structure with a total extent of 39 kpc and oriented almost along the east-west direction with the major axis

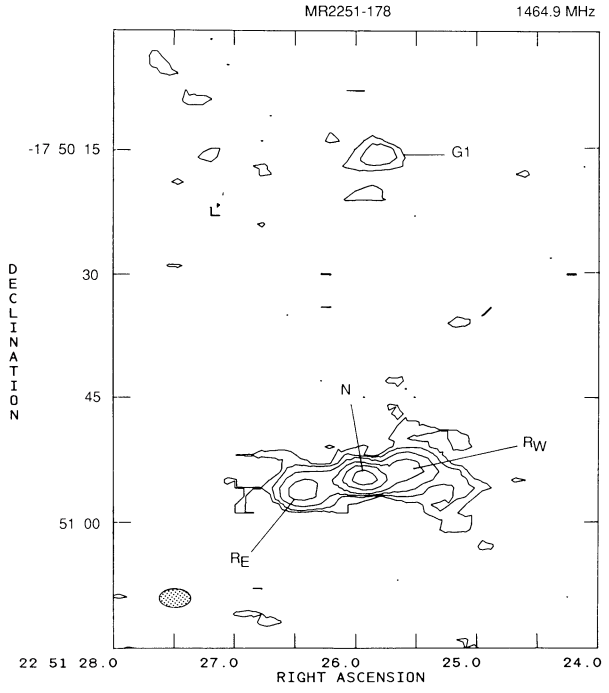

FIG. 1*a*

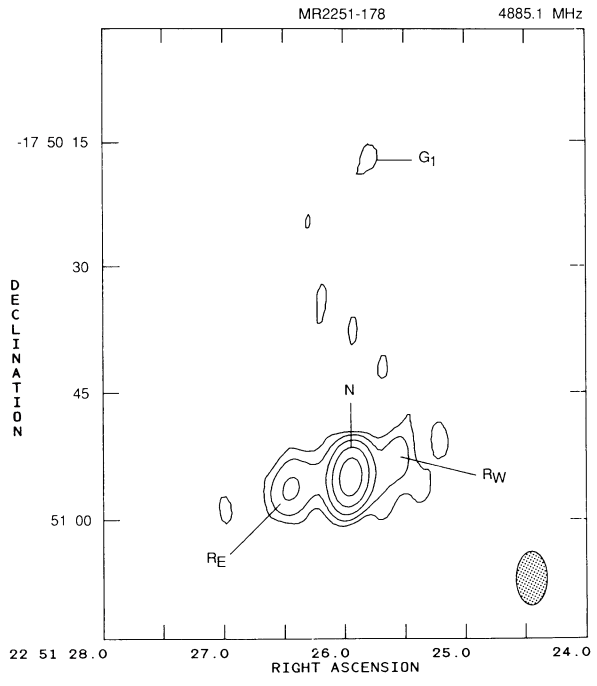

FIG. 1*b*

FIG. 1.—(*a*) VLA 20 cm map of MR 2251 − 178. The map is similar to that obtained at 6 cm except that the western component of the radio structure shows a clear bend toward the south. The peak flux corresponds to 4.4 mJy per beam and the plotted contours are at the 2%, 4%, 16%, 32%, and 64% levels of the peak. (*b*) VLA 6 cm map of MR 2251 − 178 showing central unresolved source and two faint components elongated almost along east-west direction. Also the galaxy G1, located to the north of MR 2251 − 178, is detected. The peak flux corresponds to 4.3 mJy per beam, while the plotted contours are at the 4%, 8%, 16%, 32%, and 64% levels of the peak.

TABLE 2

RADIO PROPERTIES OF MR 2251−178

Region	α	δ	*F* (6 cm) (mJy)	log *L* (6 cm) (W Hz^{-1})	*F* (20 cm) (mJy)	log *L* (20 cm) (W Hz^{-1})
Nucleus	$22^h51^m25^s.92$	−17°50′55″.7	5.48	22.99	6.68	23.07
R_E	22 51 26.44	−17 50 56.7	1101	22.25	2.50	22.64
R_W	22 51 25.56	−17 50 54.2	0.57	22.00	2.93	22.71
G1	22 51 25.78	−17 50 16.3	0.27	21.67	0.65	22.05

located at P.A. 102°. Positions and luminosities of the eastern and western components, labelled as R_E and R_W, are shown in Table 2. The luminosities were obtained measuring the flux over a surface similar in size to the beam and centered in the positions indicated in Table 2. Since the radio source is extended and the beams at 6 and 20 cm are different, no direct comparison of the 6 and 20 cm luminosities listed in Table 2 should be made to get the radio spectral index.

At 8″ from the nucleus (i.e., 15 kpc), the western component of the radio emission shows bending toward the south which is not observed in the east component. From the 20 cm radio map, the radio morphology can be considered as a typical double side jet structure, i.e., Fanaroff-Riley class I radio galaxy (Fanaroff and Riley 1974), with indications of a bending or inverse-mirror morphology.

The VLA 6 cm radio map shows an unresolved central source with two faint extensions located in the same position as the ones observed at 20 cm. Higher spatial resolution VLA 6 cm maps (Hutchings and Gower 1985) show that the central source has an elongation toward the south and a luminosity log *L* (6 cm) = 21.09 W Hz^{-1}.

The galaxy labeled as G1 (Bergeron *et al.* 1983), located at a projected distance of 75 kpc to the north of MR 2251−178, was also detected at 20 and 6 cm as a weak unresolved radio source with luminosities log *L* (20 cm) = 22.05 W Hz^{-1} and log *L* (6 cm) = 21.67 W Hz^{-1}. The spectral radio index is therefore slightly steeper than that of MR 2251−178 with $\alpha_{20}^{6} = 0.73$. No indications of the extended radio emission reported by Ricker *et al.* (1978) to be concident with this galaxy are detected in our VLA maps.

b) The Circumnuclear Emission-Line Regions

i) *The Morphological Structure*

Using our high spatial resolution CHFT images we are able to detect the presence of several emission-line regions having different excitation conditions. These regions, none of them previously detected, are well separated from the nucleus at distances between 3 kpc and 6 kpc (see Table 2 for a summary of the characteristics of these regions).

The [O III] λ5007 emission-line region reveals a bright nucleus together with an elongated circumnuclear structure following precisely the same orientation as the radio emission over a total region of 9 kpc (see Fig. 2*a* [Pl. 6]). This [O III] emission also shows two well-resolved extranuclear regions. The western component, labeled K_1 in Figure 2*a*, is located at a distance of 3.8 kpc from the nucleus and has a narrow structure elongated in the north–south direction, i.e., perpendicular to the major axis of the radio emission, over a total size of 3.6 kpc.

The eastern component, labeled K_2 in Figure 2*a*, shows a knotty structure to the southeast (P.A. 110°) at a distance of 3.2 kpc from the nucleus. Also a narrow bar, labeled as B_1 in Figure 2*a*, appears elongated along the radio emission direction all the way from the nucleus up to a distance of 5.2 kpc.

The [O II] λ3727 emission line region, i.e., low-excitation region, has a very different morphology (see Fig. 2*b*) from the [O III] region. We detect an extended, linear size of 4 kpc, and bright extranuclear region located at a distance of 3.7 kpc along the position angle P.A. 235°. Also, although less luminous, the [O II] counterpart of the [O III] K_2 knot is observed while no clear indications of the bar (B_1 in Fig. 2*a*) and the bright western knot K_1 are present.

We notice that the inner emission-line regions (within about 5 kpc from the nucleus) are strongly concentrated along the radio axis, much in a similar way to what has been observed around nearby low radio power AGN (Unger *et al.* 1987; Tadhunter and Tsvetanov 1989) and around powerful radio galaxies at high redshift (Chambers, Miley, and van Breugel 1987; McCarthy, van Breugel, and Spinrad 1987). These alignments are thought to be evidence for anisotropic ionizing radiation from the nucleus (e.g., Fosbury 1989). Also the more extended emission-line regions are confined within the two quadrants around the radio axis (see Figs. 3*a* and 3*b* [Pl. 7 and 8]).

The Hβ emission is constrained to the nuclear region, i.e., broad Hβ line, and does not show any indication of extranuclear emission (see di Serego Alighieri, Perryman, and Macchetto 1984) suggesting that the physical characteristics correspond to high excitation conditions in low dense clouds of gas.

ii) *The Physical Characteristics*

Using the luminosity measured in the [O III] emission line, we can calculate a lower limit to the density and consequently an upper limit to the total mass of ionized gas in the circumnuclear region.

Assuming that the densities are small enough for collision de-excitation effects to be unimportant (the critical density for [O III] λ5007 is $N_c = 7 \times 10^5$ cm^{-3}; Osterbrock 1989) we obtain an emissivity

$$\epsilon([\text{O III}]) = 9.79 \times 10^{-24} N_e^2 \text{ ergs cm}^{-3} \text{ s}^{-1} \quad (1)$$

considering solar abundance, an electron temperature $T = 10^4$ K and the atomic parameters as in Aller (1984).

Therefore measuring the projected size of the emission-line region and assuming a volume $V = l^{3/2}a^{3/2}$, where *l* and *a* are the projected length and width of the region in kpc, we have

$$L([\text{O III}]) = \epsilon([\text{O III}]) f l^{3/2} a^{3/2} \text{ ergs s}^{-1} \quad (2)$$

and therefore we find an electron density

$$N_e = 1.865 \times 10^{-21} L_{[\text{O III}]}^{1/2} l^{-3/4} a^{-3/4} f^{-1/2} \text{ cm}^{-3}, \quad (3)$$

where *f* is the filling factor. If $f \sim 1$ we will obtain a lower limit to the density. Consequently, considering

$$M_g = (N_p m_p + N_{\text{He}} m_{\text{He}}) f V, \quad (4)$$

$$N_{\text{He}} = 0.1 N_p \quad \text{and} \quad N_p \approx N_e, \quad (5)$$

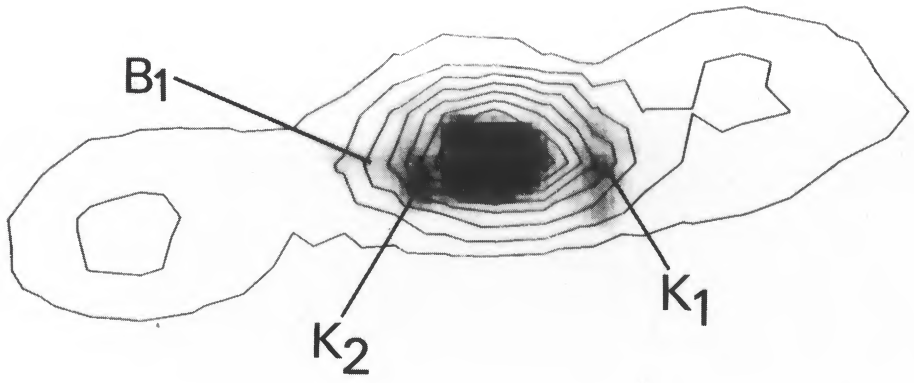

(a)

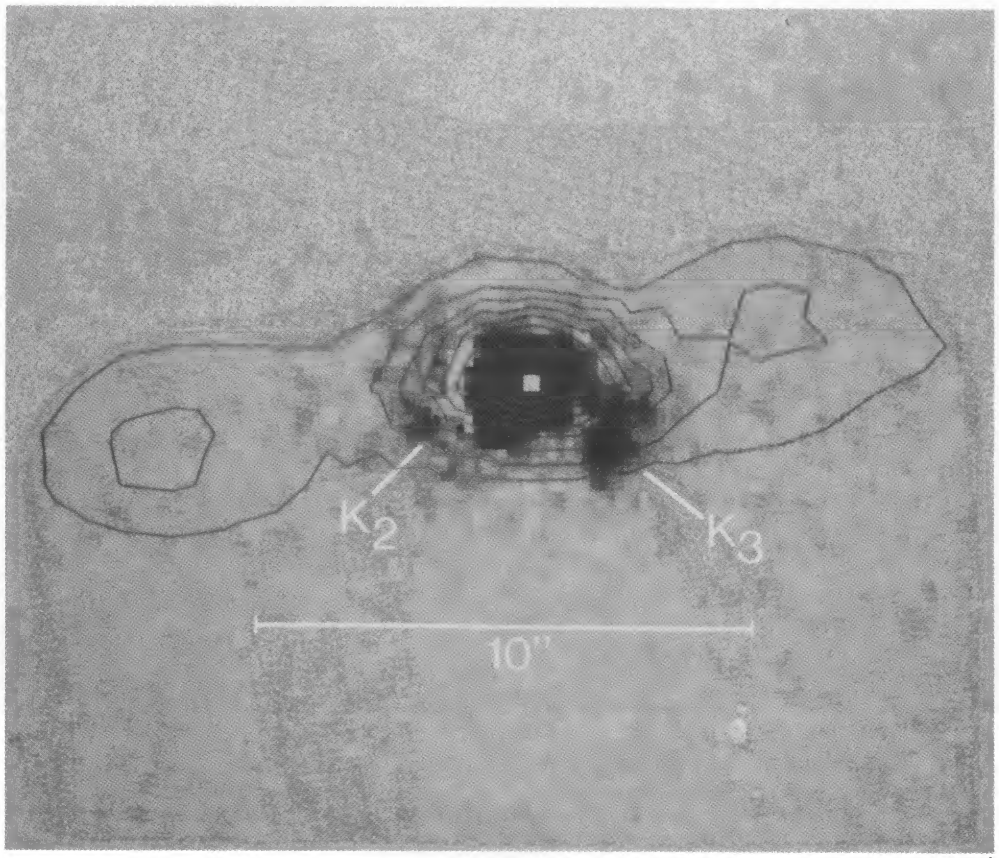

(b)

FIG. 2.—(*a*) High spatial resolution image of MR 2251 − 178 in the light of [O III] λ5007 showing the structure of the high-excitation circumnuclear gas. The VLA 20 cm radio map shows the alignment and spatial coincidence between the radio emission and the optical emission-line regions B_1 and K_1. North is at the top and east to the left. (*b*) Same high spatial resolution image as Fig. 3 but in the light of [O III] λ3727. The different structure of the low-excitation gas is clearly visible. The low-ionization regions K_2 and K_3 lie below the major axis of the radio emission. The orientation is the same as in Fig. 2*a*.

MACCHETTO *et al.* (*see* **356**, 392)

PLATE 7

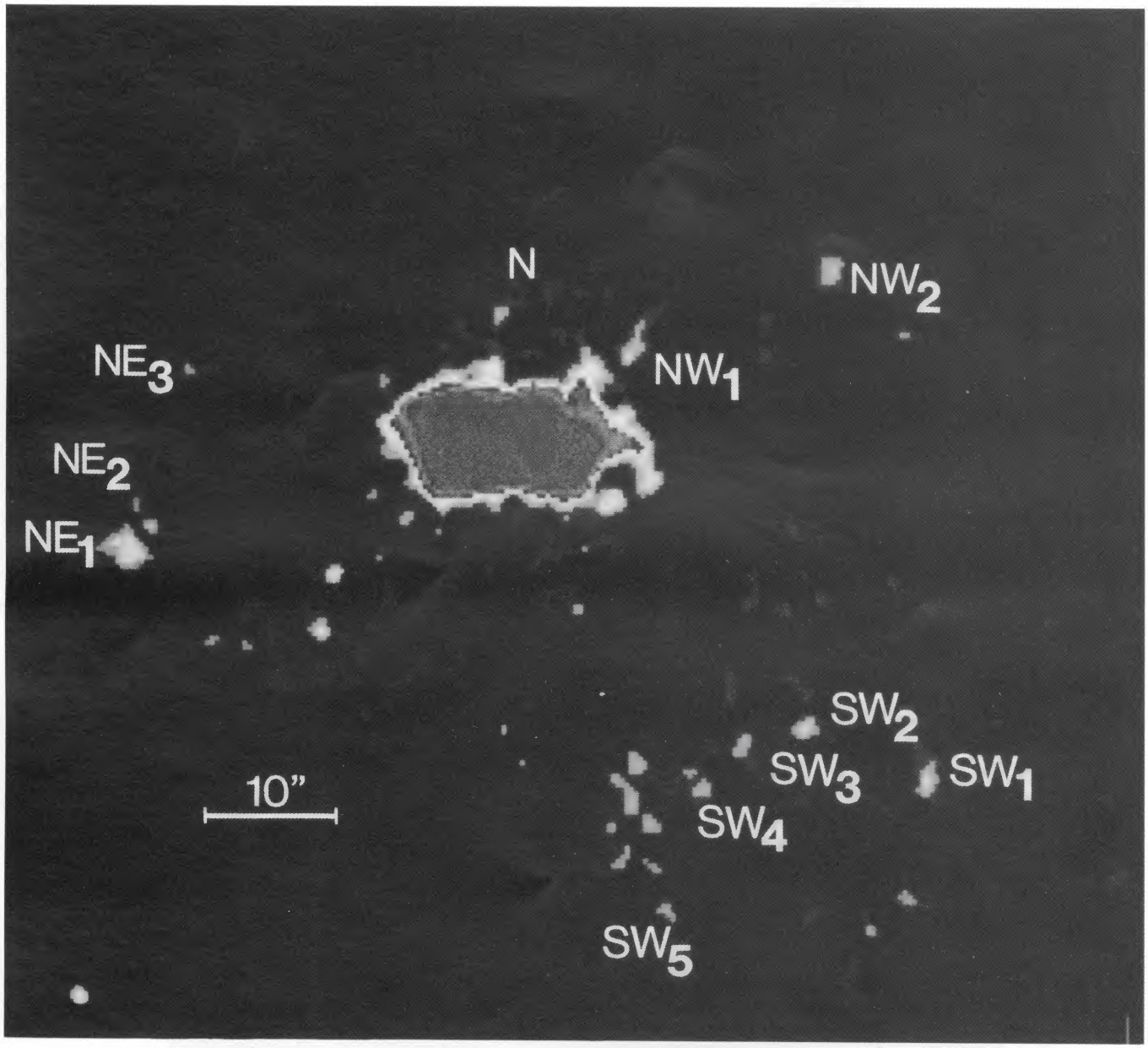

FIG. 3a

FIG. 3.—(*a*) Image of MR 2251 – 178 in the light of [O III] λ5007 showing the extended high-ionization emission filaments around MR 2251 – 178 and located at distances as far as 70 kpc from the nucleus. Note the radial symmetry of the filaments with respect to the nucleus of MR 2251 – 178. The orientation is the same as in Fig. 2. (*b*) Image of MR 2251 – 178 in the light of Hα. The two new bright filaments F_{NE} and F_E are clearly detected. Only the northern part of the filament F_{NE} is also detected in [O III] λ5007. The knots NW_1 and NW_2 represent the low-ionization counterpart of the corresponding [O III] filaments (see previous figure). The orientation is the same as in previous figures.

MACCHETTO *et al.* (*see* **356**, 392)

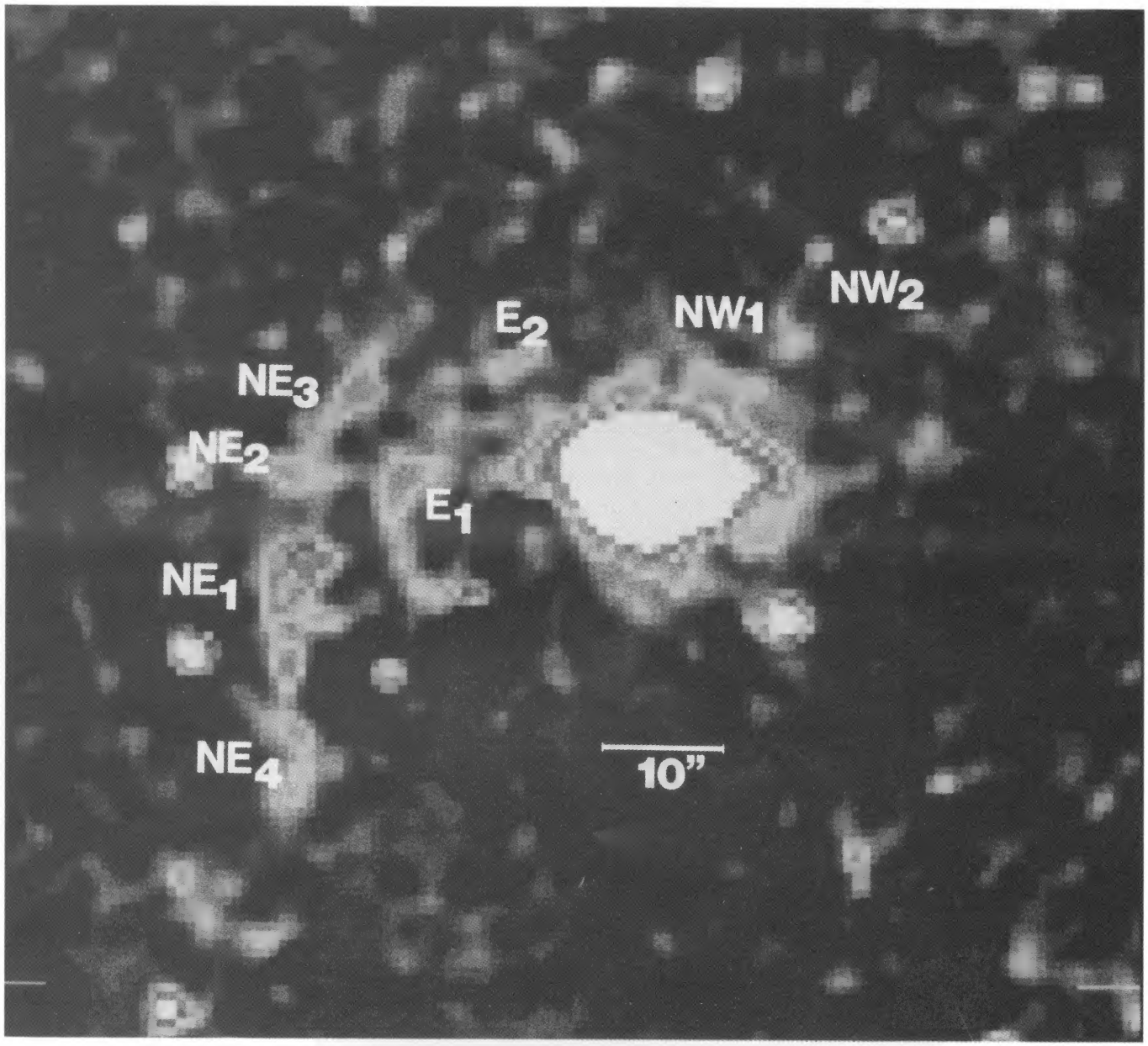

FIG. 3*b*

MACCHETTO *et al.* (*see* **356**, 392)

TABLE 3

PHYSICAL PROPERTIES OF THE CIRCUMNUCLEAR EMISSION-LINE REGIONS

Region	Size (kpc, kpc)	Distance (kpc)	L([O III] λ5007) (10^{42} ergs s^{-1})	L([O II] λ3727) (10^{42} ergs s^{-1})	N_e (cm^{-3})	Mass ($10^9 M_\odot$)	[O III]/[O II]
Nucleus	4.3, 4.3	...	7.96	1.10	...	...	...
K_1	3.6, 3.6	3.8	0.65	0.06	>0.20	<0.39	10.4
K_2	2.5, 2.5	3.2	0.41	0.02	>0.30	<0.16	21.7
B_1	3.5, 3.5	5.2	0.29	0.01	>0.15	<0.12	22.2
K_3	4.0, 4.0	3.7	0.35	0.83	>0.14	<0.30	0.42

we obtain an upper limit to the mass of ionized gas

$$M_g \leq 1.203 \times 10^{-34} L_{[\mathrm{O\ III}]} N_e^{-1} M_\odot \ . \quad (6)$$

The results, obtained from expressions (3) and (6) and considering $f \sim 1$, are represented in Table 3. Typical lower limits on the densities and upper limits on the masses lie in the range 0.1 to 0.3 cm^{-3} and 2–4 $\times$ 10^8 $M_\odot$ for each emitting region.

The ionization parameter $U = Q/4\pi r^{-2} N_e^{-1} c$ can be estimated by comparing the measured [O II] λ3727/[O III] λ5007 line ratios with the ionization parameters of detailed photoionization codes (i.e., Ferland and Netzer 1983).

The values in the knots K_1, K_2, and B_1 (see Table 3) are consistent with a high ionization parameter of the order $U \approx 10^{-2}$ which also agree with the lack of Hβ emission lines in these regions, i.e., [O III]/H$\beta \geq 10$. On the other hand, in knot K_3, where [O II] λ3727 is more luminous than [O III] λ5007, the ionization is lower by a factor of 10 or more with $U \approx 10^{-3}$.

Once we know the ionization parameter from the emission-line ratios, if the number of ionizing photons is known, we can get an upper limit to the electron density of the gas clouds, and therefore a further estimate of a lower limit to the mass.

The ionization parameter of a cloud of gas of density N_e and distance d (kpc) to the MR 2251 $-$ 178 nucleus can be written as (see § IV*b*)

$$U = 9.74 N_e^{-1} d^{-2} \ ; \quad (7)$$

we therefore obtain electron densities $N_e \leq 60$ cm^{-3} for the high excitation clouds and $N_e \leq 600$ cm^{-3} for the low-excitation cloud K_3. These densities are in good agreement with the values obtained by Bergeron and collaborators (Bergeron *et al.* 1983) from the [S II] λ6717/[S II] λ6731 emission-line ratio. They obtained $N_e \approx 300$ cm^{-3}.

Consequently, the lower limit of the mass involved in the clouds will be a factor 100–1000 smaller than the upper limit calculated previously. This means that the mass in the ionized gas is in the range 10^5 $M_\odot$–10^6 $M_\odot$. Also the filling factor will be smaller by factors 10^4–10^6, giving values similar to those found in broad-line regions (BLRs) and narrow-line regions (NLRs).

This last result can be interpreted as the mass and filling factor of the densest clouds of gas, which are also the most important contributors to the [O III] luminosity according to expression (1), and is therefore not in contradiction with the previous estimates which used a filling factor equal to one, i.e., more diffuse and less dense clouds of gas filling the whole volume.

c) The Extranuclear Extended Emission-Line Filaments

The system of extended emission-line filaments has been studied using the zoomed CFHT–PCD and EFOSC–CCD images. High ionization conditions must prevail almost everywhere since no emission in [O II] λ3727 is detected outside the central 6 kpc from the nucleus. Also no detection of Hβ in emission outside the nucleus has been reported so far (di Serego Alighieri, Perryman, and Macchetto 1984; Hansen, Nørgaard-Nielsen, and Jorgensen 1986).

i) *The Morphological Structure*

1. The [O III] Filaments

High-excitation [O III] emission-line filaments showing a knotty structure are detected at several different places and well beyond the optical and radio continuum emission (see Fig. 3*a*). We detect the following main systems (see Table 4 for a summary of the properties).

a. Filament NE.—located toward the northeast of the quasar at distances ranging from 40 kpc (knot NE_3) to 50 kpc (knot NE_1) and with a total extent of the order of 30 kpc. These

TABLE 4

PHYSICAL PROPERTIES OF THE EXTENDED [O III] EMISSION FILAMENTS

Region	Size (kpc, kpc)	Distance (kpc)	L([O III] λ5007) (10^{40} ergs s^{-1})	L([O II] λ3727) (10^{39} ergs s^{-1})	N_e (10^{-2} cm^{-3})	Mass[a] ($10^8 M_\odot$)	[O III]/[O II]
NE_1	12.1, 6.3	48.7	1.7	<1.1	>0.94	<2.0	>15.4
NE_2	11.0, 6.6	42.5	1.2	<1.1	>0.95	<1.5	>11.5
NE_3	9.2, 4.6	39.7	0.6	<0.8	>1.00	<0.7	>7.6
N_1	8.1, 2.9	16.7	0.4	<0.6	>1.10	<0.5	>6.5
N_2	13.3, 5.8	21.7	1.0	<1.1	>0.70	<1.1	>8.7
NW_1	6.3, 5.2	23.4	1.0	<0.9	>1.10	<1.2	>10.5
NW_2	6.9, 4.6	48.2	0.7	<0.7	>1.10	<0.8	>10.0
SW_1	12.7, 4.0	68.6	0.8	<0.8	>0.85	<0.9	>10.0
SW_2	6.3, 4.0	54.3	0.5	<0.6	>1.20	<0.6	>8.4
SW_3	6.3, 4.0	50.1	0.4	<0.6	>1.10	<0.5	>6.7
SW_4	8.1, 5.8	50.6	0.7	<0.8	>0.87	<0.8	>9.1
SW_5	16.1, 10.4	52.5	2.7	<1.6	>0.66	<3.3	>16.7

[a] Obtained with $N_e = 10^{-2}$ cm^{-3}.

system of knots was detected by di Serego Alighieri, Perryman, and Macchetto (1984) and Nørgaard-Nielsen *et al.* (1986).

b. Filament SW.—This system of knots is the largest and the most distant of the [O III] systems. It corresponds to the system identified as D by di Serego Alighieri, Perryman, and Macchetto (1984) and as B by Nørgaard-Nielsen *et al.* (1986), although we identify many new individual knots. It is located southwest of MR 2251−178 nucleus at distances from 50 kpc (knot SW_3) to almost 70 kpc (knot SW_1) with a total extent of almost 50 kpc.

c. Filament NW.—This system, located to the northwest of MR 2251−178, is formed by an elongated filament (labeled as NW_1) at a distance of 23 kpc and an unresolved knot (labeled as NW_2) at 48 kpc from the nucleus.

d. Filament N.—This is a new detected system of filaments at distances smaller than the previous ones. Located at a distance of around 20 kpc from the nucleus, it is formed by two elongated filaments with major axis size of 8 and 13 kpc respectively.

The first three systems of filaments are located almost radially symmetrically around the quasar suggesting an overall ring or shell morphology.

2. The Hα Filaments

Low-excitation extranuclear filaments are detected in the Hα emission line (see Fig. 3*b*). As was the case for the nuclear emission-line regions, the morphology of these low-excitation filaments is quite different from the high-excitation filaments presented in the previous section. We detect four different systems.

a. Filament NE.—Part of this filament has its high-excitation counterpart in the NE [O III] emission-line system. It is located at 50 kpc to the east of MR 2251−178. A large extension, not observed in [O III], toward the south is detected for the first time giving a total size of almost 100 kpc for this filament.

b. Filament E.—This system is also detected for the first time. It is located at a distance ranging from 25 kpc to 35 kpc from the nucleus and with a total extent of 68 kpc. It does not have a high-excitation counterpart.

c. Filament NW.—Almost at the limiting detection level of our observations, it represents the low-ionization counterpart of the NW [O III] emission filament.

d. Filament EW. This filament is elongated along the east–west direction. It is detected as a faint diffuse emission perpendicular to filaments F_{NE} and F_E, connecting them and extending all the way to the nucleus. This can be the extension of the already reported [O III] bar structure which is also coincident with the nuclear radio emission elongation.

The overall morphology of the Hα filaments is reminiscent of a spiral galaxy with very well defined arms.

ii) *The Physical Characteristics*

1. The [O III] Filaments

In order to estimate the physical parameters of the [O III] system of filaments we have followed the same procedure outlined in § III*b*ii. Using expressions (3) and (6) we get typical density values of $N_e \geq 10^{-2}$ cm^{-3} and upper limit of the masses ranging from 5×10^7 to $2 \times 10^8\ M_\odot$ in each individual knot of gas. The upper limit to the total amount of gas in the [O III] system is $M_T \leq 1.5 \times 10^9\ M_\odot$ (see Table 4 for detailed results).

The ionization conditions are very high since the [O II] λ3727 and Hβ were not detected. However if we estimate the upper limit to the [O II] luminosity in the filaments, we obtain [O III]/[O II] ratios of the order of 10 or larger. This is consistent with a high ionization parameter $U \approx 10^{-2}$. This value is typical of the extended emission line regions (EELR) recently discovered in Seyfert galaxies (Unger *et al.* 1987; Wilson, Ward, and Haniff 1988) and higher than those usually measured in extended emission regions around powerful radio galaxies (Baum and Heckman 1989).

Using equation (7) and the previous estimate of the ionization parameter we obtain an upper limit to the electron density $N_e \approx 0.4$–1 cm^{-3} and consequently a lower limit to the mass. Following equations (6) and (3) the mass will be lower by a factor of 100 with respect to the calculated upper limit and the filling factor will be 10^{-4}.

2. The Hα Filaments

For the low-excitation emission-line filaments, we have obtained the lower limit on the density and upper limit on the mass by using the Hα luminosity and assuming case B recombination. Consequently,

$$\epsilon(\mathrm{H}\alpha) = N_p N_e \alpha_{\mathrm{H}\alpha}^{\mathrm{eff}} h\nu_{\mathrm{H}\alpha} = 3.544 \times 10^{-25} N_e^2 \text{ ergs cm}^{-3}\text{ s}^{-1}\,, \tag{8}$$

assuming $\alpha_{\mathrm{H}\alpha}^{\mathrm{eff}} = 1.17 \times 10^{-13}$ cm^3 s^{-1} for $T_e = 10^4$ K (Spitzer 1968). Therefore, following the same arguments as in § III*b*i we obtain

$$N_e = 9.798 \times 10^{-21} L_{\mathrm{H}\alpha}^{1/2} l^{3/4} a^{3/4} f^{-1/2} \text{ cm}^{-3} \tag{9}$$

and assuming $f \sim 1$,

$$M_g \leq 3.321 \times 10^{-33} L_{\mathrm{H}\alpha} N_e^{-1}\ M_\odot\,. \tag{10}$$

The results for $f \sim 1$ and expressions (9) and (10) are shown in Table 5. The density value are in agreement with those

TABLE 5

PHYSICAL PROPERTIES OF THE EXTENDED Hα EMISSION FILAMENTS

Region	Size (kpc, kpc)	Distance (kpc)	L(Hα) (10^4 ergs s^{-1})	L([O III] λ5007) 10^{40} ergs s^{-1}	N_e 10^{-2} cm^{-2}	Mass[a] $10^9\ M_\odot$	[O III]/Hα
NE_1	15.1, 15.1	53.2	0.7	1.7	>2.2	<2.2	2.5
NE_2	11.3, 11.3	47.7	0.6	1.2	>3.1	<2.1	2.0
NE_3	11.3, 11.3	40.9	0.7	0.6	>2.1	<2.2	0.9
NE_4	15.1, 15.1	51.7	1.0	<0.3	>1.7	<3.2	<0.3
F_{NE}	96.6, 13.8	51.0	6.2	3.8	>1.1	<21	0.61
E_1	11.3, 11.3	33.9	0.7	≤0.6	>2.3	<2.3	≤0.9
E_2	8.8, 8.8	25.4	0.3	≤0.2	>3.6	<1.0	≤0.8
F_E	67.8, 11.3	30.0	2.8	≤1.3	>1.1	<9.3	≤0.5
NW_1	11.3, 11.3	46.0	0.2	0.7	>1.2	<0.7	3.0
NW_2	11.3, 11.3	27.5	0.4	0.9	>1.6	<1.3	2.3

[a] Obtained using $N_e = 10^{-2}$ cm^{-3}.

obtained from the [O III] luminosity with typical values in the range 0.01 to $0.02e^-$ cm^{-3}. The mass in these low-excitation clouds are a factor of 10 larger than that measured in the high-excitation filaments given a total mass $M_T(\mathrm{H}\alpha) \leq 3.2 \times 10^{10} M_\odot$.

The ionization conditions can be estimated from the [O III]/Hβ ratio obtained from the [O III]/Hα ratio and assuming Hα/Hβ = 2.86 according to case B recombination theory for an electron temperature $T_e = 10^4$ K (Aller 1984). Using this method we get [O III]/Hβ ratios which are of the order of 6 to 8 for those filaments clearly detected in [O III] and of the order of 1 to 2 for those where only very faint [O III] or upper limits where derived.

Comparing these values with the expected results from ionization codes (Ferland and Netzer 1983), we obtain very low ionization parameters ranging from 10^{-4} to 10^{-3}. If this result is correct we should expect [O II]/[O III] ≥ 1. Therefore, we should observe extended [O II] emission-line filaments in our [O II] image and this is not the case. For the filaments where [O III] is also detected, we get, from the [O III]/Hβ ratio, an ionization parameter an order of magnitude smaller than the one derived from the [O II]/[O III] line ratio.

This discrepancy is most likely understood in terms of the uncertainties in our absolute calibration and in the physical conditions in the EELRs. These effects make it very difficult to get any reliable value of the ionization parameter using the [O III]/Hβ ratio. Further discrepancies may result from a possible oxygen underabundance and from the [N II] contribution to the Hα line emission under low ionization conditions.

Bergeron and collaborators (1983) suggest that the oxygen in the extended filaments has an abundance 0.3 solar. If correct, this effect will produce a decrease in the [O III]/Hβ value while leaving the [O II]/[O III] ratio almost unchanged (see Ferland and Netzer 1983 to compare models with different abundances).

On the other hand, since the [N II] $\lambda\lambda$6548, 6584 lines lie within our narrow-band Hα filter, an important effect could also be due to the contribution of the [N II] flux. In estimating the Hα flux, and therefore the luminosities listed in Table 5, we considered the [N II]/Hα values obtained for the extended emission by Bergeron *et al.* (1983). This [N II] flux, amounting to a total of 0.36 times the Hα flux, was obtained from long-slit spectroscopy and therefore does not map the ionization gradients in different regions. Besides, the [N II] λ6584 flux could be equal to or even larger than that of the Hα line if an ionization parameter of the order of 10^{-3} or less is present in these regions (see, e.g., Ferland and Netzer 1983). This means that under low ionization conditions, the Hα luminosities could be smaller by a factor of 2, thereby increasing the [O III]/Hβ ratio by the same quantity.

IV. DISCUSSION

a) *The Ionizing Source*

All detected galaxies showing EELRs larger than a few kpc are either powerful radio sources with P(1.4 GHz) $\geq 1.3 \times 10^{25}$ ergs s^{-1} Hz^{-1} (Baum and Heckman 1989; Fosbury 1989) or luminous quasars with $M_v \leq -24.7$ (Stockton and MacKenty 1987). These types of galaxies are therefore brighter than MR 2251−178 by at least an order of magnitude in optical and/or radio luminosity. In this respect MR 2251−178 represents a unique example of a low-redshift intermediate luminous active galaxy with an EELR sharing the physical properties of those detected around very luminous active galaxies.

Could the central nonthermal source of MR 2251−178 ionize the whole system of filaments? Or do we need to invoke the presence of a local ionizing source to explain the detected line luminosities? In the following we will explore the different alternatives regarding the ionizing source.

i) *The Radio Jet*

Since many of the EELRs around powerful radio galaxies are spatially coincident with the radio structure, a physical connection between the two phenomena has been suggested in some cases (see van Breugel 1989 for a review). In particular, direct heating and ionization by relativistic particles could increase the emission-line luminosity (Ferland and Mushotzky 1984). Also star formation produced by the direct interaction between the radio jet and the ambient gas has been claimed (van Breugel *et al.* 1985; Brodie, Bowyer, and McCarthy 1985; Rees 1989).

These local effects are not sufficient to explain the extranuclear extended system of emission-line filaments around MR 2251−178 since they are located well beyond the radio emission regions and at different angular positions.

We can also rule out this mechanism to explain the luminosities of the circumnuclear emission-line regions. First, ionization effects due to relativistic particles are very small compared to ionization due to photons. In these regions near the nonthermal UV nucleus the photon density, and therefore the ionization parameter, is very high (see Ferland and Mushotzky 1984 or Wilson, Ward, and Haniff 1988 for a detailed discussion). Second, it could be that the emission-line luminosities were generated in shocks due to the entrainment of the radio jet with the interstellar medium. Although this mechanism could be energetically feasible if the kinetic energy in the flow is E_k(flow) $\approx 10^{44}$ ergs s^{-1} (see Wilson *et al.* for a discussion on the efficiency factors from kinetic to emission line and radio luminosities conversion), the line ratios expected from even high velocity shocks do not fit with the lack of Hβ in emission, ie.., with the high [O III]/Hβ values and the low [O II]/[O III] ratios (see Binette, Dopita, and Tuohy 1985).

ii) *Cluster of Hot Stars*

The presence of a cluster of young stars, i.e., a giant H II region, could be an alternative local ionizing source which can not be ruled out based only on our luminosity measurements. If no internal extinction effects are important in these filaments, Hα/Hβ ratios in agreement with case B recombination theory have been measured in the extended nebulosity (Bergerson *et al.* 1983), one can obtain the amount of ionizing photons in a particular Hα knot or filament using the Hα luminosity and considering case B recombination:

$$N_{\mathrm{ph}} = \frac{\alpha_B(H^o, T)}{\alpha_{\mathrm{eff}}^{\mathrm{H}\alpha}(T)} \times \frac{L(\mathrm{H}\alpha)}{h\nu_{\mathrm{H}\alpha}} \qquad (11)$$

where $\alpha_B = 2.59 \times 10^{-13}$ cm^3 s^{-1} (Osterbrock 1989) and $\alpha_{\mathrm{H}\alpha}^{\mathrm{eff}} = 1.17 \times 10^{-13}$ cm^3 s^{-1} (Spitzer 1968). For $T_e = 10^4$ K, we obtain the number of ionizing photons

$$N_{\mathrm{ph}} = 7.30 \times 10^{11} L(\mathrm{H}\alpha)\,, \qquad (12)$$

where L(Hα) is the Hα luminosity in ergs s^{-1}. For a typical luminosity range of 10^{39}–10^{40} ergs s^{-1} in the Hα emission-line knots, we get a value of N_{ph} in the range 10^{51}–10^{52} ph s^{-1}. Considering blue young stars (O8) characterized by an effective

temperature $T_{\rm effect}({\rm O8}) \approx 3.5 \times 10^4$ K and $N_{\rm ph}({\rm O8}) \approx 4 \times 10^{48}$ ph s^{-1} (Osterbrock 1989), a cluster of at least 10^3 stars are needed to account for the observed Hα luminosities if the covering factor is unity. In this case, assuming an absolute magnitude $M_V({\rm O8}) = -5.2$ (Osterbrock 1989) we get $m_V = 25.2$ for such a cluster of stars at the redshift of MR 2251−178. This apparent magnitude is below our detection limit in the V image.

If the covering factor is less than unity, but not much less since we are considering a local ionizing source, we would need up to 10 times more O8 stars in order to explain the Hα luminosities. In this case the apparent magnitude of such a cluster would be $m_V \approx 23$ which should be visible in our CCD image.

On the other hand, if most of the ionizing photons come from very hot stars ($T \approx 10^5$ K), one needs very few of these stars to ionize the gas and produce the observed luminosities and the stars will be invisible at optical wavelengths. Such stars could also explain high excitation conditions as those in the [O III] filaments. In fact the ionizing radiation produced by a blackbody characterized by a temperature $T_{\rm bb} \approx 10^5$ K can explain the observed line spectra in active galaxies (Binette, Robinson, and Courvoisier 1988).

iii) *Central Non-thermal Source*

Since most of the filaments are well detected in [O III] λ5007 (ionization potential of O^{++} is equal to 35.12 eV), this means that high-excitation conditions prevail everywhere. Therefore, a hard UV nonthermal source can be used to explain the line luminosities. If a spectral index $\alpha = -1$ is used to extrapolate the observed UV flux [$F_\nu(\lambda 1400) \approx 2 \times 10^{-26}$ ergs s^{-1} cm^{-2} Hz^{-1}, Bergeron *et al.*] and an isotropic radiating power law source ($F_\nu \propto \nu^{+\alpha}$) is assumed, we obtain the number of ionizing photons:

$$N_{\rm ph} \approx 4\pi D^2 F_\nu(\lambda 912)(h\alpha)^{-1} = 3.4 \times 10^{55} \text{ ph} \cdot \text{s}^{-1} , \quad (13)$$

where D is the distance between MR 2251−178 and us. Therefore, adding together the line luminosities in the different filaments, only a few percent of the total available ionizing UV photons are used for this purpose indicating that the covering factor of the gas is rather small or that the gas is optically thin to the radiation.

On the other hand, once we know the number of ionizing photons, we can calculate the ionization parameter for a certain cloud at an estimated distance d (in kpc) to the nucleus and with a certain density N_e (in cm^{-3}). Considering expression (13) we have

$$U = N_{\rm ph}(4\pi)^{-1} c\, d^{-2} N_e^{-1} = 9.74\, d^{-2} N_e^{-1} . \quad (14)$$

As shown in §§ III*b*ii and III*c*ii, the measured U values obtained from the emission-line ratios are also consistent with that expected from the previous formula if the electron density is of the order of 10^2 cm^{-3} in the circumnuclear regions and of the order of 0.5 cm^{-3} in the extended filaments.

b) The Origin of the Gas

Based on the morphology and kinematics of the EELRs, scenarios like cooling flows, interactions, or mergers between galaxies have been invoked to explain the origin of the gas around radio galaxies (Tadhunter, Fosbury, and Quinn 1989; Heckman *et al.* 1986). In the following we attempt to define the most likely hypothesis in MR 2251−178.

i) *Cooling Flows*

There are several arguments against the existence of a cooling flow around MR 2251−178.

i. Although MR 2251−178 seems to belong to a small group/cluster of galaxies, both its location, far from the geometrical center of the cluster, and its velocity, located in the low-velocity tail of the cluster velocity distribution (Bergeron *et al.* 1983), are not characteristic of a massive elliptical galaxy lying in the minimum of the cluster potential well.

ii. Cooling flows appear centrally concentrated around the giant elliptical galaxy and with sizes of the order of 5 kpc (Heckman *et al.* 1989). In MR 2251−178 the system of filaments is radially located at distances as large as 70 kpc and with filaments as large as 100 kpc in size.

iii. Incomplete kinematical information (Bergeron *et al.* 1983) indicates a clear rotation pattern close to the nucleus up to 6 kpc and at distances larger than that, a flat rotation curve. This is also incompatible with recent results by Heckman and colllaborators (Heckman *et al.* 1989). Their kinematical results for a number of cooling flows provide no evidence for rotational motions.

iv. X-ray observations of MR 2251−178 (Cooke *et al.* 1978) detect variations by factors up to 10 within short time scales. This suggests that most of the X-ray emission is generated in the nucleus of the galaxy and not in a huge hot envelope hundreds of kpc in size.

ii) *Cold Gas Envelope*

This scenario has been suggested by Bergeron and collaborators (1983). They hypothesized that the detected system of filaments could be part of a giant H I envelope surrounding MR 2251−178. Based on the flattening observed in the velocity field at large distances from the nucleus, they concluded that the total mass within a radius of 170 kpc should be $M_T = 1.3 \times 10^{12} \sin^{-2} i\, M_\odot$, where i is the inclination of the galaxy. Considering $i = 40°$ (di Serego, Alighieri, Perryman, and Macchetto 1984), a total mass $M_T = 3.2 \times 10^{12}\, M_\odot$ is obtained.

If a large fraction of this mass is in the form of neutral hydrogen, the envelope is more massive than typical H I envelopes around Seyfert galaxies (Heckman, Balick, and Sullivan 1978). So far, only in the nearby Seyfert 2 galaxy Mrk 348 a clear detection of a huge H I envelope with a size of 100 kpc in radius and a mass of $3 \times 10^{10}\, M_\odot$ has been made. If the hypothesis of this very massive H I envelope is correct, one should be able to detect it in the H I 21 cm line observations.

iii) *Interaction/Merging Remnant*

The hypothesis of the interaction or merging remnant is favored for the following reasons.

i. The morphology of the radio jet shows a bend to the southwest and whole structure has indications of inverse-mirror symmetry. This morphology appears mostly in low-luminosity radio galaxies with nearby companions (Shaver *et al.* 1982; Colina and Pérez-Fournon 1990) and is explained as consequence of tidal interactions (Wirth, Smarr, and Gallagher 1982). Also precessional effects in a system of two nuclear black holes originated by the merger of two galaxies (Begelman, Blandford, and Rees 1980; Gower *et al.* 1982) could produce such morphology.

ii. Similar morphologies of the EELRs as the one detected in MR 2251−178 have been observed around some powerful radio galaxies (Tadhunter, Fosbury, and Quinn 1989 and references). These galaxies show an overall ring or disk struc-

ture together with a rotation curve velocity field. This could be interpreted as a result of a recent merger where the gas is settling into a disk located in the plane of the interaction and bound to MR 2251−178 (see also di Serego Alighieri *et al.* 1986). In fact, a rotation curve velocity pattern has been measured by Bergeron and collaborators (1983) at distances of few kpcs.

iii. The upper limit to the ionized mass, $M_T \leq 10^{10}\ M_\odot$, obtained from our data has a value which is consistent with the idea that a gas-rich spiral galaxy merged with the elliptical galaxy hosting MR 2251−178.

c) *Suggested Overall Scenarios*

i) *Past Interaction with Galaxy G1*

This idea was first suggested by di Serego Alighieri and collaborators (1984). In their picture it was assumed that a gravitational interaction occurred between MR 2251−178 and the galaxy G1 some 2×10^8 years ago. It was also assumed that the ionized gas around MR 2251−178 was a small part of a huge H I gas envelope bound to MR 2251−178 as suggested by Bergeron and collaborators (1983). Under this scheme, galaxy G1 passed through the envelope producing shocks and generating, as a consequence, the inhomogeneities of the gaseous envelope. Furthermore, the interaction was able to generate a luminous active nucleus in MR 2251−178 and a low-ionization nuclear emission-line region (LINER) type activity in the galaxy G1. The fact that G1 holds a weak active nucleus is also supported by our detection of G1 as a radio source at 6 and 20 cm (see § III*a*).

It has been demonstrated that close passages, distances of the order of 20 kpc, of companion galaxies could induce Seyfert-type activity in the nucleus of a galaxy (Byrd *et al.* 1986). Also, in many groups around Seyfert galaxies appear companion galaxies showing low luminous active nucleus (Fricke and Kollatschny 1989).

Considering the absolute magnitudes of G1 and the MR 2251−178 galaxy (Hansen, Nørgaad-Nielsen, and Jorgensen 1986) and assuming that the same mass-luminosity ratio holds for both galaxies, we conclude that MR 2251−178 is 5 times more massive than G1. Also the relative velocity between them, $V_{\rm rel} = 1246$ km s^{-1} (Bergeron *et al.* 1983), is very large. Therefore, on the hypothesis of a highly hyperbolic encounter between MR 2251−178 and G1, since tidal forces are directly proportional to the mass of the companion and inversely proportional to the third power of the distance, and the interaction time scale in this particular case is much smaller than the orbital time scale ($T_{\rm int}/T_{\rm orb} \approx V_{\rm orb}/V_{\rm rel}$), the integrated gravitational effect could be important enough to start the fueling of a dormant blackhole in the nucleus of MR 2251−178 but not sufficient to substantially distort the stellar and gas distribution in the envelope.

ii) *Merger Remnant*

A second scenario considers that MR 2251−178 and its associated system of emission-line filaments are the result of a merger between a giant elliptical galaxy (MR 2251−178) and a smaller gas-rich spiral galaxy. In this case, the system of filaments with its highly symmetric ring morphology would be a consequence of the merging process. Also, the observed VLA radio morphology could be explained as a precessional motion of the radio source in the orbital field of a pair of blackholes (Begelman, Blandford, and Rees 1980). This system of black holes could exist in the nucleus of MR 2251−178 as a result of the merging process since, as demonstrated by Balcells and Quinn (1989), the nucleus of a galaxy with a mass even 10 times smaller than that of the giant galaxy could survive the whole merging process.

If this idea is correct, one should detect giant stellar shell structures like those seen around nearby elliptical galaxies (Malin and Carter 1980). These shells are usually rather faint in surface brightness, between 27 and 30 mag arcsec^{-2} (Malin and Carter 1980); therefore they are well below our present detection limit in the V band.

These structures have been successfully explained as density enhancements produced by a low angular momentum encounter between a massive elliptical galaxy and a small gas-rich disk galaxy (Quinn 1984; Hernquist and Quinn 1987) and have also been observed in some of the radio galaxies showing a disk/ring emission-line structure similar to that of MR 2251−178 (see Tadhunter, Fosbury, and Quinn 1989).

This scenario makes some predictions which could be checked with the *Hubble Space Telescope* (HST). The first one is the presence, at distances of few tens of kpcs, of faint stellar shell structures. If they exist and are equally bright in surface brightness to those detected in nearby galaxies (Malin and Carter 1980), the apparent magnitude will be fainter and could be detected only with the wide field planetary camera (WFPC) of the *HST*. The second prediction is related to the presence of a pair of black holes located at the nucleus of MR 2251−178. If the two black holes are still separated by a hundred parsecs (wide binary; Begelman, Blandford, and Rees 1980), one might be able to detect two cusps of light with the high spatial resolution (at the MR 2251−178 redshift $0\farcs1 = 95h_0^{-1}$ parsecs where $h_0 = H_0/100$) provided by the faint object camera (FOC) of the *HST*. The presence of displaced emission peaks in the broad emission-line profiles with respect to the systemic host galaxy velocity has also been interpreted as the existence of a binary black hole in the nucleus of the galaxy (Gaskell 1988). This effect might also be checked with high-resolution high S/N spectra.

V. SUMMARY

The detection of new systems of [O II] λ3727, [O III] λ5007, and Hα filaments is reported. The circumnuclear gas is located at distances between 3 and 6 kpc from the nucleus, with an upper mass limit of $10^8\ M_\odot$ and ionization conditions consistent with direct excitation by the nonthermal central source. These inner emission-line regions are strongly concentrated around the radio axis in a way similar to what is observed in some Seyfert galaxies and high-redshift radio galaxies.

The whole extranuclear system of filaments has an overall disk/ring structure at typical distance of 50–70 kpc. The upper limit on the mass of the ionized gas is of the order of $10^{10}\ M_\odot$. The high-excitation conditions observed in these filaments can be explained by the hard UV ionizing flux coming from the nonthermal nucleus of MR 2251−178.

Two overall scenarios to explain both the activity of MR 2251−178 and the origin of the gas are outlined. The first one suggest the past interaction between MR 2251−178 and the galaxy G1 located to the north. Although G1 is 5 times less massive than MR 2251−178 and their relative velocity is in excess of 1000 km s^{-1}, a close hyperbolic passage could activate both galaxies without affecting the envelope.

In the second picture, the system of filaments are the remnant of a past merger between the elliptical MR 2251−178 host galaxy and a smaller gas-rich galaxy. This scenario makes

two predictions: the presence of faint stellar shells at distances of the order of few tens of kpcs, and the existence of a nuclear pair of black holes also expected as remnants of the merger.

MR 2251−178 is an unique example of weak radio galaxy showing a system of emission-line filaments similar in its physical characteristics (e.g., density, luminosity, mass, alignment) to those detected around powerful radio galaxies.

Luis Colina acknowledges the support of the European Space Agency under an ESA Postdoctoral Fellowship. The observations reported in this paper were obtained at the CFHT, ESO, and VLA. We wish to thank these observatories for their support. In particular we wish to thank J.-L. Nieto and G. Lelièvre who helped us during the CFHT observations.

REFERENCES

Aller, L. H. 1984, *Physics of Thermal Gaseous Nebulae* (Dordrecht: Reidel).
Balcells, M., and Quinn, P. 1989, preprint.
Baum, S. A., and Heckman, T. M. 1989, *Ap. J.*, **336**, 681.
Begelman, M. C., Blandford, R. D., and Rees, M. J. 1980, *Nature*, **287**, 307.
Bergeron, J., Boksenberg, A., Dennefeld, M., and Tarenghi, M. 1983, *M.N.R.A.S.*, **202**, 125.
Binette, L., Dopita, M. A., and Tuohy, I. R. 1985, *Ap. J.*, **297**, 476.
Binette, L., Robinson, A., Courvoisier, T. J. L. 1988, *Astr. Ap.*, **194**, 65.
Brodie, J. P., Bowyer, S., and McCarthy, P. 1985, *Ap. J. (Letters)*, **293**, L59.
Byrd, G. G., Valtonen, M., Sundelius, B., and Valtaja, L. 1986, *Astr. Ap.*, **166**, 75.
Chambers, K. C., Miley, G. K., and van Breugel, W. 1987, *Nature* **329**, 604.
Colina, L., and Pérez-Fournon, I. 1990, *Ap. J. Suppl.*, **70**, 41.
Cooke, B. A., *et al.* 1978, *M.N.R.A.S.*, **182**, 489.
di Serego Alighieri, S., Perryman, M. A. C., and Macchetto, F. 1984, *Ap. J.*, **285**, 567.
———. 1985, *Astr. Ap.*, **149**, 179.
di Serego Alighieri, S., Perryman, M. A. C., Macchetto, F. Nieto, J. L., and Lelièvre, G. 1986, *Bull. Astr. Soc. India*, **14**, 180.
Fanaroff, B. L., and Riley, F. M. 1974, *M.N.R.A.S.*, **167**, 31P.
Ferland, G. J., and Mushotzky, R. F. 1984, *Ap. J.*, **286**, 42.
Ferland, G. J., and Netzer, H. 1983, *Ap. J.*, **264**, 105.
Fosbury, R. A. E. 1989, in *Proc. ESO Workshop on Extranuclear Activity in Galaxies*, ed. E. J. A. Meurs and R. A. E. Fosbury (Garching: ESO), p. 169.
Fricke, K. J., and Kollatschny, W. 1989, *IAU Symposium 134, Active Galactic Nuclei*, ed. D. E. Osterbrock and J. S. Miller, (Dordrecht: Reidel), p. 425.
Gaskell, C. M. 1988, *Proc. Georgia State University Conf. Active Galactic Nuclei*, ed. H. R. Miller and P. J. Wiita (Berlin: Springer), p. 61.
Gower, A. C., Gregory, P. C., Hutchings, J. B., and Unruh, W. G. 1982, *Ap. J.*, **262**, 478.
Hansen, L., Nørgaard-Nielsen, H. U., and Jorgensen, H. E. 1984, *Astr. Ap.*, **136**, L11.
Heckman, T. M., Balick, B., and Sullivan, W. T., III 1978, *Ap. J.*, **224**, 745.
Heckman, T. M., Baum, S. A., van Breugel, W. J. M., and McCarthy, P. 1989, *Ap. J.*, **338**, 48.
Heckman, T. M., Smith, E. P., Baum, S. A., van Breugel, W. Miley, G. K. Illingworth, G. D., Bothun, G. D., and Balick, B. 1986, *Ap. J.*, **311**, 526.
Hernquist, L., and Quinn, P. J. 1987, *Ap. J.*, **312**, 1.
Hutchings, J. B., and Campbell, B. 1983, *Nature*, **303**, 583.
Hutchings, J. B., Crampton, D., Campbell, B., Duncan, D., and Glendenning, B. 1984, *Ap. J. Suppl.*, **55**, 319.
Hutchings, J. B., and Gower, A. C. 1985, *A.J.*, **90**, 405.
Kembhavi, A., Feigelson, E. D., and Singh, K. P. 1986, *M.N.R.A.S.*, **220**, 51.
Malin, D. F., and Carter, D. 1980, *Nature*, **285**, 643.
McCarthy, P. J., van Breugel, W., and Spinrad, H. 1987, *Ap. J. Letters*), **321**, L29.
Nørgaard-Nielsen, H. U., Hansen, L., Jorgensen, H. E., and Christensen, P. R. 1986, *Astr. Ap.*, **169**, 49.
Osterbrock, D. E. 1989, *Astrophysics of Gaseous Nebula and Active Galactic Nuclei* (Mill Valley: University Science Books).
Quinn, P. J. 1984, *Ap. J.*, **279**, 596.
Rees, M. 1989, *M.N.R.A.S.*, **239**, 1P.
Ricker, G. R., Clarke, G. W., Doxley, R. E., Dower, R. G., Jernigan, J. G., Delvaille, J. P., MacAlpine, G. M., and Hjellming, R. M. 1978, *Nature*, **271**, 35.
Shaver, P. A., Danziger, I. J., Ekers, R. D., Fosbury, R. A. E., Goss, W. M., Malin, D., Moorwood, A. F. M., and Wall, J. V. 1982, in *IAU Symposium 97, Extragalactic Radio Sources*, ed. D. J. Heeschen and C. M. Wade (Dordrecht: Reidel), p. 55.
Spitzer, L. 1968, *Diffuse Matter in Space* (New York: Wiley).
Stockton, A., and MacKenty, J. W. 1987, *Ap. J.*, **316**, 584.
Tadhunter, C. N., Fosbury, R. A. E., and Quinn, P. J. 1989, *M.N.R.A.S.*, **240**, 225.
Tadhunter, C. N., and Tsvetanov, Z. 1989, *Nature*, **341**, 422.
Unger, S. W., Pedlar, A., Axon, D. J., Whittle, M., Meurs, E. J. A., and Ward, M. J. 1987, *M.N.R.A.S.*, **238**, 671.
van Breugel, W. 1989, *Proc. Ringberg Conference on Hot Spots in Extragalactic Radio Sources*, ed. K. Meisenheimer and H. J. Röser (Berlin: Springer), in press.
van Breugel, W., Filippenko, A. V., Heckman, T. M., and Miley, G. K. 1985, *Ap. J.*, **293**, 83.
Wilson, A. S., Ward, M. J., and Haniff, C. A. 1988, *Ap. J.*, **334**, 121.
Wirth, A., Smarr, L., and Gallagher, J. S. 1982, *A.J.*, **87**, 602.

L. Colina, D. Golombek, and F. Macchetto: Space Telescope Institute, 3700 San Martin Drive, Homewood Campus, Baltimore, MD 21218

S. di Serego Alighieri: Space Telescope European Coordinating Facility, Karl-Schwarzschild-Str. 2, D-8046 Garching bei Muñchen, Federal Republic of Germany

M. A. C. Perryman: Astrophysics Division, Space Science Department of ESA, ESTEC, Postbus 299, NL-2200 AG, Noordwijk, The Netherlands.